Single spin asymmetries in elastic electron-nucleon scattering

B. Pasquini[1,2] and M. Vanderhaeghen[3,4]

[1] Dipartimento di Fisica Nucleare e Teorica, Università degli Studi di Pavia and INFN, Sezione di Pavia, Pavia, Italy
[2] ECT*, Villazzano (Trento), Italy
[3] Thomas Jefferson National Accelerator Facility, Newport News, VA 23606, USA,
[4] Department of Physics, College of William and Mary, Williamsburg, VA 23187, USA

Abstract. We discuss the target and beam normal spin asymmetries in elastic electron-nucleon scattering which depend on the imaginary part of two-photon exchange processes between electron and nucleon. In particular, we estimate these transverse spin asymmetries for beam energies below 2 GeV, where the two-photon exchange process is dominated from the resonance contribution to the doubly virtual Compton scattering tensor on the nucleon.

PACS. 25.30.Bf Elastic electron scattering – 25.30.Rw Electroproduction reactions

1 Introduction

Elastic electron-nucleon scattering in the one-photon exchange approximation is a valuable tool to access information on the structure of hadrons. New experimental techniques exploiting polarization observables have made possible precision measurements of hadron structure quantities, such as its electroweak form factors, parity violating effects, $N \to \Delta$ transition form factors, and spin dependent structure functions. However, to push the precision frontier further in electron scattering, one needs a good control of 2γ exchange mechanisms and needs to understand how they may affect different observables. The imaginary (absorptive) part of the 2γ exchange amplitude can be accessed through a single spin asymmetry (SSA) in elastic electron-nucleon scattering, when either the target or beam spin are polarized normal to the scattering plane. As time reversal invariance forces this SSA to vanish for one-photon exchange, it is of order $\alpha = e^2/(4\pi) \simeq 1/137$. Furthermore, to polarize an ultra-relativistic particle in the direction normal to its momentum involves a suppression factor m/E (with m the mass and E the energy of the particle), which typically is of order $10^{-4} - 10^{-3}$ when the electron beam energy is in the 1 GeV range. Therefore, the resulting target normal SSA can be expected to be of order 10^{-2}, whereas the beam normal SSA is of order $10^{-6} - 10^{-5}$. In the case of a polarized lepton beam, asymmetries of the order ppm are currently accessible in parity violation (PV) elastic electron-nucleon scattering experiments. While the PV asymmetry measurements involve a beam spin polarized along its momentum, the SSA for an electron beam spin normal to the scattering plane can be accessed using the same experimental apparatus. Results from first measurements of this beam normal SSA have

been presented in this conference.

Model calculations for such observables have been recently performed in different kinematical regimes [1,2,3,4]. Here we report a study of the imaginary part of the 2γ exchange entering in the normal SSA's at low and intermediate beam energies [5]. Using unitarity, one can relate the imaginary part of the 2γ amplitude to the electroabsorption amplitudes on a nucleon. Below or around two-pion production threshold, one is in a regime where these electroproduction amplitudes are relatively well known using pion electroproduction experiments as input. Therefore the aim is to gain a good knowledge of the imaginary part of the two-photon exchange amplitude, and then to use such information as input for dispersion relations which will allow to quantify the contribution of the real part of the 2γ exchange processes. In addition, observables such as normal SSA's are sensitive to the electroproduction amplitudes on the nucleon for a wide range of photon virtualities. This may provide information on resonance transition form factors complementary to the information obtained from pion electroproduction experiments.

2 Single spin asymmetries in elastic electron-nucleon scattering

The target spin asymmetries in elastic electron-nucleon scattering is defined by

$$A_n = \frac{\sigma_\uparrow - \sigma_\downarrow}{\sigma_\uparrow + \sigma_\downarrow}, \tag{1}$$

where $\sigma_\uparrow$ ($\sigma_\downarrow$) denotes the cross section for an unpolarized beam and for a nucleon spin parallel (anti-parallel) to the

normal polarization vector $\boldsymbol{S}_n = (\boldsymbol{k} \times \boldsymbol{k}')/|\boldsymbol{k} \times \boldsymbol{k}'|$ (with $\boldsymbol{k}$ and $\boldsymbol{k}'$ the three-momenta of the initial and final electron, respectively). Analogous expression as in Eq. (1) holds for the beam spin asymmetry (B_n) when we interpret $\sigma_\uparrow$ $(\sigma_\downarrow)$ as the cross section for an unpolarized target and for an electron beam spin parallel (antiparallel) to the normal polarization vector. As has been shown by de Rujula et $al.$ [6], the target and beam normal spin asymmetry are related to the absorptive part of the elastic eN scattering amplitude. Since the one-photon exchange amplitude is purely real, the leading contribution to SSA's is of order $O(e^2)$, and is due to an interference between one- and two-photon exchange amplitudes, i.e.

$$\text{SSA} = \frac{2 \, \text{Im}(\sum_{spins} T_{1\gamma}^* \cdot \text{Abs} \, T_{2\gamma})}{\sum_{spins} |T_{1\gamma}|^2}, \qquad (2)$$

where $T_{1\gamma}$ is the one-photon exchange amplitude, and Abs $T_{2\gamma}$ is the absorptive part of the doubly virtual Compton scattering tensor on the nucleon, as shown in Fig. 1.
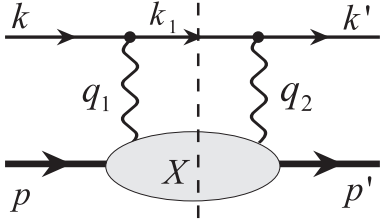

Fig. 1. The 2γ exchange diagram. The blob represents the response of the nucleon to the scattering of the virtual photon.

Eq. (2) can be expressed in terms of a 3-dimensional phase-space integral as

$$\text{SSA} = -\frac{1}{(2\pi)^3} \frac{e^2 Q^2}{D(s,Q^2)} \int_{M^2}^{(\sqrt{s}-m_e)^2} dW^2 \frac{|\boldsymbol{k}_1|}{4\sqrt{s}}$$
$$\times \int d\Omega_{k_1} \frac{1}{Q_1^2 Q_2^2} \text{Im} \left\{ L_{\alpha\mu\nu} H^{\alpha\mu\nu} \right\}, \qquad (3)$$

where $W^2 = p_X^2$ is the squared invariant mass of the intermediate state X, and $s = (p+k)^2$. In Eq. (3), the momenta are defined as in Fig. 1, $Q_1^2 \equiv -q_1^2$ and $Q_2^2 \equiv -q_2^2$ correspond with the virtualities of the two spacelike photons, $D(s,Q^2) \equiv Q^4/e^4 \sum_{spins} |T_{1\gamma}|^2$, and $L_{\alpha\mu\nu}$ and $H^{\alpha\mu\nu}$ are the leptonic and hadronic tensors, respectively. Furthermore, Eq. (3) reduces to the target or beam asymmetry once we specify the helicities for the polarized particles and take the sum over the helicities of the unpolarized particles. The explicit expression for the tensor $H^{\alpha\mu\nu}$ is given by :

$$H^{\alpha\mu\nu} = W^{\mu\nu} \cdot [\bar{u}(p', \lambda'_N) \Gamma^\alpha(p', p) u(p, \lambda_N)]^*, \qquad (4)$$

where $\Gamma^\alpha(p', p)$ is the elastic photon-nucleon vertex and $W^{\mu\nu}$ corresponds with the absorptive part of the doubly

virtual Compton scattering tensor with two *spacelike* photons. The latter is given by

$$W^{\mu\nu}(p', \lambda'_N; p, \lambda_N) = \sum_X (2\pi)^4 \, \delta^4(p + q_1 - p_X)$$
$$\times < p' \, \lambda'_N |J^{\dagger\mu}(0)|X> < X|J^\nu(0)|p \, \lambda_N >, \qquad (5)$$

where the sum goes over all possible *on-shell* intermediate hadronic states X. The number of intermediate states X which one considers in the calculation sets a limit on how high in energy one can reliably calculate the hadronic tensor in Eq. (5). In addition to the elastic contribution $(X = N)$ which is exactly calculable in terms of on-shell nucleon electromagnetic form factors, we approximate the remaining inelastic part of $W^{\mu\nu}$ with a sum over all πN intermediate states (i.e. $X = \pi N$ in the blob of Fig. 1). The calculation is performed by using the unitarity relation which allows to express $W^{\mu\nu}$ in terms of electroabsorption amplitudes $\gamma^* N \to X$ at different photon virtualities. To estimate the pion electroproduction amplitudes we use the phenomenological MAID analysis (version 2000) [7], which contains both resonant and non-resonant pion production mechanisms. This same strategy has been used before in the description of real and virtual Compton scattering in the resonance region, and checked against data in Ref. [8].

3 Results and discussion

In this section we show our results for both beam and target normal spin asymmetries for elastic electron-proton scattering. Our calculation covers the whole resonance region, and addresses measurements performed or in progress at MIT-Bates [9], MAMI [10], JLab [11,12], and SLAC [13]. In Fig. 2, we show the beam normal spin asymmetry B_n for elastic $e^{-\uparrow}p \to e^- p$ scattering at a low beam energy of $E_e = 0.2$ GeV. At this energy, the elastic contribution is sizeable. The inelastic contribution is dominated by the region of threshold pion production, as is shown in Fig. 3, where we display the integrand of the W-integration for B_n. When integrating the full curve in Fig. 3 over W, one obtains the total inelastic contribution to B_n (i.e. dashed-dotted curve in Fig. 2). The present calculation (MAID) of the threshold pion electroproduction is consistent with chiral symmetry predictions, and is therefore largely model independent. One notices that at backward *c.m.* angles (i.e. with increasing Q^2) the $\pi^+ n$ and $\pi^0 p$ intermediate states contribute with opposite sign. The peaked structure at the maximum possible value of the integration range in W, i.e. $W_{max} = \sqrt{s} - m_e$, is due to the near singularity (in the electron mass) corresponding with quasi-real Compton scattering (RCS), in which both photons in the 2γ exchange process become quasi-real. This contribution at large W mainly drives the results for the inelastic part of the beam asymmetry. Furthermore, it is seen from Fig. 2 that the inelastic and elastic contributions at a low energy of 0.2 GeV have opposite sign, resulting in quite a small asymmetry. It is somewhat puzzling that the only experimental data point at this energy
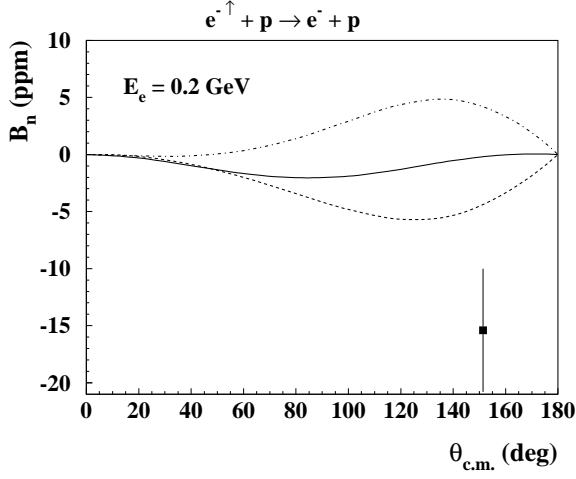
Fig. 2. Beam normal spin asymmetry B_n for $e^{-\uparrow}p \rightarrow e^-p$ at a beam energy $E_e = 0.2$ GeV as function of the *c.m.* scattering angle, for different hadronic intermediate states (X) in the blob of Fig. 1 : N (dashed curve), πN (dashed-dotted curve), sum of the N and πN (solid curve). The data point is from the SAMPLE Collaboration (MIT-Bates) [9].
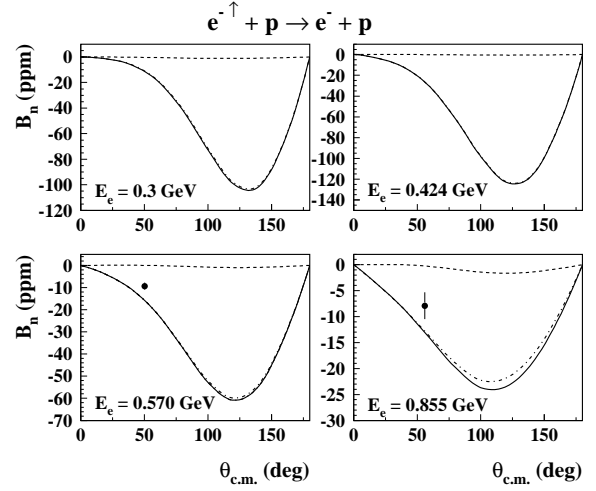

Fig. 4. Beam normal spin asymmetry B_n for $e^{-\uparrow}p \rightarrow e^-p$ as function of the *c.m.* scattering angle at different beam energies, as indicated on the figure. The meaning of the different lines is the same as in Fig. 2. The data points are from the A4 Collaboration (MAMI) [10].
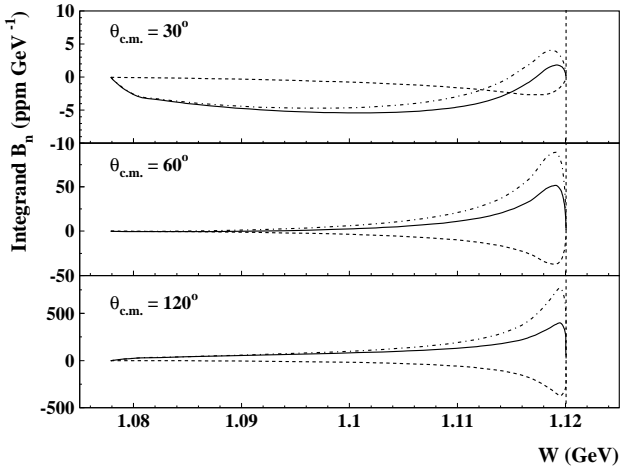

Fig. 3. Integrand in W of the beam normal spin asymmetry B_n for $e^{-\uparrow}p \rightarrow e^-p$ at a beam energy of $E_e = 0.2$ GeV and at different *c.m.* scattering angles as indicated on the figure. The dashed curves are the contribution from the $\pi^0 p$ channel, the dashed-dotted curves show the contribution from the $\pi^+ n$ channel, and the solid curves are the sum of the contributions from the $\pi^+ n$ and $\pi^0 p$ channels. The vertical dashed line indicates the upper limit of the W integration, i.e. $W_{max} = \sqrt{s} - m_e$.

indicates a larger negative value at backward angles, although with quite large error bar.

In Fig. 4, we show B_n at different beam energies below $E_e = 1$ GeV. It is clearly seen that at energies $E_e = 0.3$ GeV and higher the elastic contribution yields only a very small relative contribution. Therefore B_n is a direct
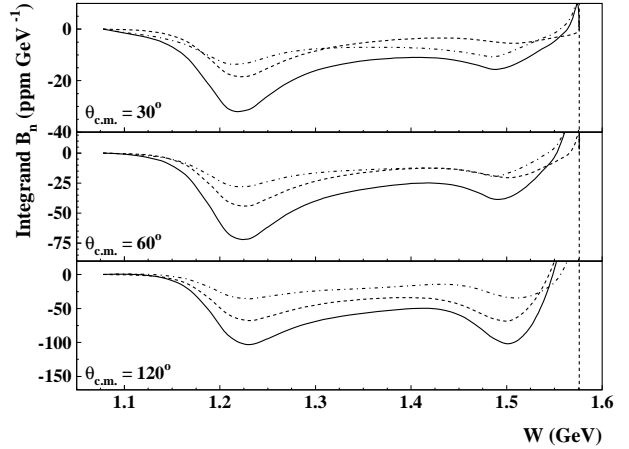

Fig. 5. Integrand in W of the beam normal spin asymmetry B_n for $e^{-\uparrow}p \rightarrow e^-p$ at a beam energy of $E_e = 0.855$ GeV and at different *c.m.* scattering angles as indicated on the figure. The meaning of the different lines is the same as in Fig. 3.

measure of the inelastic part which gives rise to sizeable large asymmetries, of the order of several tens of ppm in the backward angular range. At forward angles, the size of the predicted asymmetries is compatible with the first high precision measurements performed at MAMI. It will be worthwhile to investigate if the slight overprediction (in absolute value) of B_n, in particular at $E_e = 0.57$ GeV, is also seen in a backward angle measurement, which is planned in the near future at MAMI.

To gain a better understanding of how the inelastic contribution to B_n arises, we show in Fig. 5 the integrand
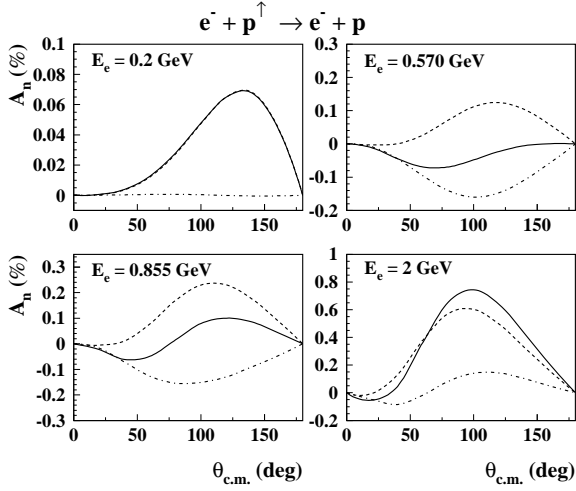
Fig. 6. Target normal spin asymmetry A_n for $e^-p^\uparrow \to e^-p$ as function of the $c.m.$ scattering angle at different beam energies, as indicated on the figure. The meaning of the different lines is the same as in Fig. 2.

Fig. 7. Integrand in W of the target normal spin asymmetry A_n for $e^-p^\uparrow \to e^-p$ for a beam energy of $E_e = 0.855$ GeV and at different $c.m.$ scattering angles as indicated on the figure. The meaning of the different lines is the same as in Fig. 3.

of B_n at $E_e = 0.855$ GeV and at different scattering angles. The resonance structure is clearly reflected in the integrands for both π^+n and π^0p channels. At forward angles, the quasi-RCS at the endpoint $W = W_{max}$ only yields a very small contribution, which grows larger when going to backward angles. This quasi-RCS contribution is of opposite sign as the remainder of the integrand, and therefore determines the position of the maximum (absolute) value of B_n when going to backward angles.

We next discuss the target normal spin asymmetry A_n. In Fig. 6, we show the results for both elastic and inelastic contributions to A_n at different beam energies. At a low beam energy of $E_e = 0.2$ GeV, A_n is completely dominated by the elastic contribution. Going to higher beam energies, the inelastic contribution becomes of comparable magnitude as the elastic one. This is in contrast with the situation for B_n where the elastic contribution already becomes negligible for beam energies around $E_e = 0.3$ GeV. The integrand of the inelastic contribution at a beam energy of $E_e = 0.855$ GeV is shown in Fig. 7. The total inelastic result displays a π^+n threshold region contribution and a peak at the $\Delta(1232)$ resonance. Notice that the higher resonance region is suppressed in comparison with the corresponding integrand for B_n. Also the quasi-RCS peak around the maximum W value is absent. As a result, the elastic contribution to A_n can be of comparable magnitude as the inelastic one. Due to the partial cancellation between elastic and inelastic contributions, A_n is significantly reduced for the proton, taking on values around or below 0.1 % for beam energies below 1 GeV.

4 Conclusions

In this contribution, we presented calculations for beam and target normal SSAs in the kinematics where several
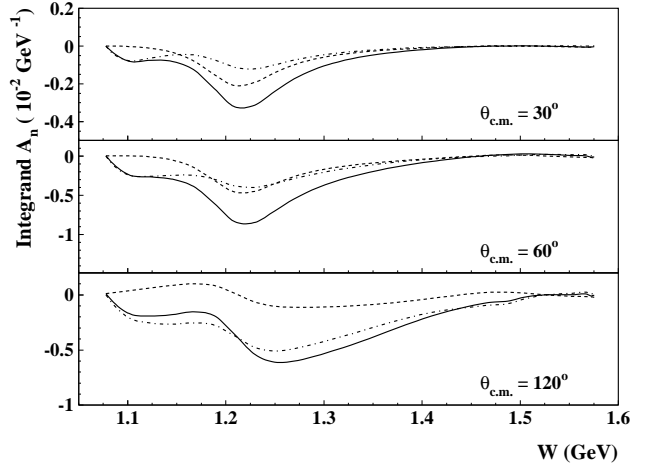
experiments are performed or in progress.

Besides providing estimates for ongoing experiments, this work can be considered as a first step in the construction of a dispersion formalism for elastic electron-nucleon scattering amplitudes. In such a formalism, one needs a precise knowledge of the imaginary part as input in order to construct the real part as a dispersion integral over this imaginary part. The real part of the two-photon exchange amplitudes may yield corrections to elastic electron-nucleon scattering observables, such as the unpolarized cross sections or double polarization observables. Therefore it is of primary importance to quantify this piece of information, in order to increase the precision in the extraction of hadron structure quantities such as the nucleon form factors.

References

1. A.V. Afanasev, et al., hep-ph/0208260.
2. A.V. Afanasev, and N.P. Merenkov, Phys. Lett. **B 599** (2004) 48.
3. M. Gorchtein, et al., Nucl. Phys. **A 741** (2004) 234.
4. L. Diaconescu, M.J. Ramsey-Musolf, nucl-th/0405044.
5. B. Pasquini, and M. Vanderhaeghen, hep-ph/0405303.
6. A. De Rujula, et al., Nucl. Phys. **B 35** (1971) 365.
7. D. Drechsel, et al., Nucl. Phys. **A645** (1999) 145.
8. D. Drechsel, et al., Phys. Rep. **378** (2003) 99.
9. S.P. Wells *et al.* (SAMPLE Coll.), Phys. Rev. C **63** (2001) 064001.
10. F. Maas *et al.* (MAMI/A4 Coll.), nucl-ex/0410013.
11. JLab HAPPEX-2 experiment (E-99-115), spokespersons G. Cates, K. Kumar, D. Lhuillier.
12. JLab G0 experiment (E-00-006, E-01-116), spokesperson D. Beck.
13. SLAC E158 experiment, contact person K. Kumar.